entropy

MDPI

Article

Effects of Movable-Baffle on Heat Transfer and Entropy Generation in a Cavity Saturated by CNT Suspensions: Three-Dimensional Modeling

Abdullah A.A.A. Al-Rashed [1], Walid Aich [2,3], Lioua Kolsi [2,4], Omid Mahian [5,*], Ahmed Kadhim Hussein [6] and Mohamed Naceur Borjini [4]

1 Department of Automotive and Marine Engineering Technology, College of Technological Studies, The Public Authority of Applied Education and Training, 13092 Kuwait City, Kuwait; aa.alrashed@paaet.edu.kw
2 College of Engineering, Mechanical Engineering Department, Haïl University, 2440 Haïl City, Saudi Arabia; w.aich@uoh.edu.sa (W.A.); l.kolsi@uoh.edu.sa (L.K.)
3 Unité de Recherche Matériaux, Energie et Energies Renouvelables MEER, Faculté des Sciences de Gafsa, Sidi Ahmed Zarroug, 2112 Gafsa, Tunisia
4 Unité de Recherche de Métrologie et des Systèmes Energétiques, Ecole Nationale d'Ingénieurs, University of Monastir, 5000 Monastir, Tunisia; borjinimn@yahoo.com
5 Renewable Energies, Magnetism and Nanotechnology Lab, Faculty of Science, Ferdowsi University of Mashhad, 9187147578 Mashhad, Iran
6 Mechanical Engineering Department, College of Engineering, Babylon University, 51002 Babylon City, Iraq; ahmedkadhim7474@gmail.com
* Correspondence: omid.mahian@gmail.com; Tel.: +98-915-770-3880

Academic Editor: Kevin H. Knuth
Received: 3 March 2017; Accepted: 26 April 2017; Published: 29 April 2017

Abstract: Convective heat transfer and entropy generation in a 3D closed cavity, equipped with adiabatic-driven baffle and filled with CNT (carbon nanotube)-water nanofluid, are numerically investigated for a range of Rayleigh numbers from 10^3 to 10^5. This research is conducted for three configurations; fixed baffle (V = 0), rotating baffle clockwise (V+) and rotating baffle counterclockwise (V−) and a range of CNT concentrations from 0 to 15%. Governing equations are formulated using potential vector vorticity formulation in its three-dimensional form, then solved by the finite volume method. The effects of motion direction of the inserted driven baffle and CNT concentration on heat transfer and entropy generation are studied. It was observed that for low Rayleigh numbers, the motion of the driven baffle enhances heat transfer regardless of its direction and the CNT concentration effect is negligible. However, with an increasing Rayleigh number, adding driven baffle increases the heat transfer only when it moves in the direction of the decreasing temperature gradient; elsewhere, convective heat transfer cannot be enhanced due to flow blockage at the corners of the baffle.

Keywords: computational fluid dynamics (CFD); convection; entropy; nanofluids; driven baffle; 3D

1. Introduction

Mixed convection heat transfer can be found in many industrial and engineering applications such as electronic component cooling, the food drying process, nuclear reactors, chemical processing equipment and so on. Several heat transfer enhancement techniques have been used to make efficient thermal devices by improving their thermal performance. For convective heat transfer, the increase of the effective surface area is one of the ways to ameliorate the heat transfer rate but it leads to an increase of the manufacturing cost. Removing this problem can be achievable by using a water-based nanofluid

and inserts to generate the swirl in the bulk of the fluids and disturb the actual boundary layer, resulting in an increase of the effective surface area, residence time and consequently the convective heat transfer coefficient in the existing system. Nanofluids are stable suspension of the nanoparticles in a base fluid such as water, ethylene glycol and industrial oils. Nanoparticles can be metallic such as Copper and Silver, metal oxide such as CuO and Al_2O_3 and nonmetallic such as carbon nanotubes (CNT) and SiC [1]. Nanofluids have been applied in many energy systems, especially renewable energy-based systems [2–4].

A sizable amount of research interests has been addressed in the last decades on natural and mixed convection in 2D nanofluid-filled cavities. The effect of different nanofluid on the entropy generation in 2D porous cavity was studied numerically by Ashorynejad and Hoseinpour [5]. In addition to the type of nanofluids, authors investigated the porosity and volume fraction of nanoparticles. The main result was that entropy generation is increasing with porosity and is decreasing with the nanoparticle volume fraction for all type of nanofluids. Cianfrini et al. [6] carried out a numerical study on the effect of the length and the position of the heater on nanofluid laminar natural convection inside a partially heated square cavity. Based on the obtained results and in addition to the flow structure and temperature field, authors presented correlations for the Nusselt number. A numerical study was conducted by Wang et al. [7] on 2D natural convection of a square enclosure with cooled right vertical wall. The left vertical wall was sinusoidally oscillated at the constant average temperature of the cavity with adiabatic horizontal walls. The cavity was filled by nanofluid, and the effect of the nanofluid volume fraction on heat transfer was the paramount objective of this research. The conclusions drawn show that the heat transfer and the oscillating behaviors were influenced by nanoparticles. Sheikhzadeh et al. [8] analyzed numerically a 2D steady laminar natural convection heat transfer and flow patterns of Cu-water nanofluid in a cavity with partially active vertical walls, while the horizontal walls were assumed to be thermally insulated. Authors concluded that heat transfer increases with increasing both the Rayleigh number and nanoparticle volume fraction. A magnetohydrodynamics (MHD) mixed convection of nanofluid in a 2D lid-driven square cavity that contains a rotating cylinder was simulated numerically by Selimefendigil and Öztop [9]. The main objective was the investigation of the effects of the dimensionless parameters such as the Hartmann number, Richardson number, rotational speed of the cylinder, and the concentration of the nanoparticles. It was found that an increasing Richardson number leads to an increment of heat transfer. However, by increasing the value of the Hartmann number, heat transfer is reduced. Rotation of the cylinder has a considerable effect on the heat transfer enhancement. A 2D mixed convection nanofluid flow in an enclosure with moving top wall and wavy bottom wall was numerically investigated by Abu-Nada and Chamkha [10]. It was proved that at the considered *Ri*, the nanoparticles have a significant effect on the heat transfer enhancement as well as the wavy bottom wall geometry ratios.

As mixed convection in industrial/chemical applications is often turbulent, recent development in the field of entropy generation and irreversibility in buoyancy-driven convection was achieved. Zonta et al. [11] performed DNS (Direct Numerical Simulations) to evaluate NOB (Non-Oberbeck–Boussinesq) effects on momentum and heat transfer mechanisms for stably-stratified turbulence in water flows. They have demonstrated that, for all situations in which NOB effects become significant, the Reynolds analogy is not justified and accurate physical modeling is required to improve parameterization of mixing. In another work, Zonta et al. [12] have analyzed the behavior of entropy fluctuations in turbulent thermal convection; they have performed DNS of a turbulent Rayleigh–Bénard flow inside a vertically confined fluid layer and they have followed the dynamics of pointwise Lagrangian tracers to measure the local quantities of the flow. They have shown that entropy production can be evaluated by looking at the work done by buoyancy on fluid particles.

The above presented literature survey shows that the majority of numerical investigations are restricted to the two-dimensional geometry and only very limited work has been done on 3D lid-driven cavity problems [13–15]. Furthermore, no attention has been paid to mixed convection in three-dimensional closed cavities with inserted driven baffle. This paper aims to undertake a

comprehensive analysis of the flow patterns and temperature distributions of mixed convection heat transfer in a 3D enclosure filled with CNT-water nanofluid and equipped with adiabatic-driven baffle.

2. Physical Problem and Governing Equations

The main cubic geometry parameters are sketched in Figure 1. As shown, the left side of the closed space has a higher temperature than the right side while other walls are assumed to be insulated. The adiabatic baffle inserted on the top wall is allowed to rotate clockwise or counterclockwise with uniform velocity. The enclosure is filled with CNT/water nanofluid and the mixed convection flow is a result of movement of the adiabatic-driven baffle and the temperature gradient.

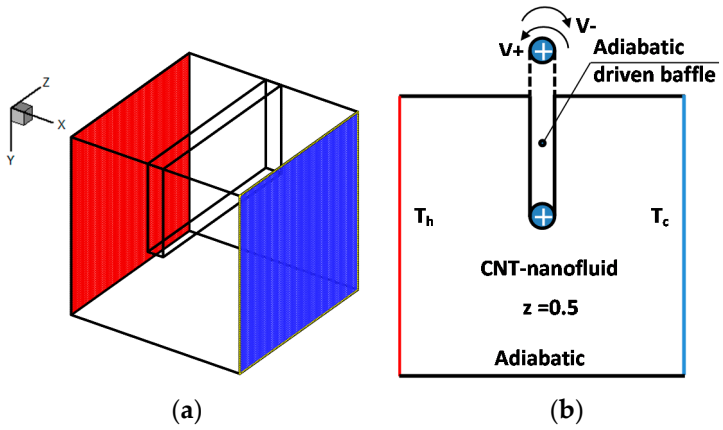

Figure 1. Schematic diagram of the considered configuration. (**a**) 3D geometry, (**b**) central plane ($z = 0.5$).

The nanofluid is assumed to be incompressible and the flow is considered laminar. The base fluid and nanoparticles are assumed to be at thermal equilibrium. Table 1 presents the thermo-physical properties of the base fluid (water) and the nanoparticles.

Table 1. Thermo-physical properties of water and carbon nanotube (CNT) nanoparticles at 25 °C.

Property	Water	CNT
C_p (J/kg·K)	4179	650
ρ (kg/m^3)	997.1	1350
k (W/m·K)	0.613	3500
β (1/K)	1×10^{-5}	4.2×10^{-5}
v (mm^2/s)	0.8926	–

2.1. Governing Equations

As a numerical method, we had recourse to the potential vector–vorticity formalism $(\vec{\psi} - \vec{\omega})$ which allows, in a 3D configuration, the elimination of the pressure, which is a delicate term to treat [16,17]. To eliminate this term, one applies the rotational to the equation of momentum. The potential vector and the vorticity are, respectively, defined by the two following relations:

$$\vec{\omega'} = \vec{\nabla} \times \vec{V'} \text{ and } \vec{V'} = \vec{\nabla} \times \vec{\psi'} \quad (1)$$

The governing equations are written in non-dimensional forms as:

$$-\vec{\omega} = \nabla^2 \vec{\psi} \quad (2)$$

$$\frac{\partial \vec{\omega}}{\partial t} + (\vec{V} \cdot \nabla)\vec{\omega} = (\vec{\omega} \cdot \nabla)\vec{V} + \frac{\nu_{nf}}{\nu_f}\mathrm{Pr} \cdot \nabla^2\vec{\omega} - \frac{\beta_{nf}}{\beta_f}Ra\mathrm{Pr}\vec{\nabla} \times T\vec{g} \tag{3}$$

$$\frac{\partial T}{\partial t} + \vec{V} \cdot \nabla T = \frac{\alpha_{nf}}{\alpha_f}\nabla^2 T \tag{4}$$

The time (t'), velocity ($\vec{V'}$), vector potential ($\vec{\psi'}$) and vorticity ($\vec{\omega'}$), are put respectively in their dimensional forms by l^2/α, α/l, α and l^2/α. The non-dimensional temperature is defined by:

$$T = (T' - T'_c)/(T'_h - T'_c) \tag{5}$$

Prandtl and Rayleigh numbers are defined respectively as:

$$\mathrm{Pr} = \frac{\nu}{\alpha} \text{ and } Ra = \frac{g \cdot \beta \cdot \Delta T \cdot l^3}{\nu \cdot \alpha} \tag{6}$$

In addition, the Richardson number is defined as:

$$Ri = \frac{Gr}{\mathrm{Re}^2} = \frac{Ra}{\mathrm{Pr} \cdot \mathrm{Re}^2} \tag{7}$$

The effective density of the nanofluid is given by Kahveci [18] as:

$$\rho_{nf} = (1 - \varphi)\rho_f + \varphi\rho_s \tag{8}$$

The heat capacitance of the nanofluid is expressed by Kahveci [16] as:

$$(\rho C_p)_{nf} = (1 - \varphi)(\rho C_p)_f + \varphi(\rho C_p)_s \tag{9}$$

The effective thermal conductivity of the nanofluid is approximated by Xue [19] as:

$$\frac{k_{nf}}{k_f} = \frac{1 - \varphi + 2\varphi\frac{k_s}{k_s - k_f}\ln\left(\frac{k_s + k_f}{2k_f}\right)}{1 - \varphi + 2\varphi\frac{k_f}{k_s - k_f}\ln\left(\frac{k_s + k_f}{2k_f}\right)} \tag{10}$$

The effective dynamic viscosity of the nanofluid is given by the Brinkman model [20] as:

$$\mu_{nf} = \frac{\mu_f}{(1 - \varphi)^{2.5}} \tag{11}$$

2.2. Boundary Conditions

The boundary conditions for the present problem are given as follows:

- Temperature:

  $T = 0$ at $x = 0$, and $T = 1$ $x = 1$;

  $\frac{\partial T}{\partial n} = 0$ at all other walls (i.e., adiabatic).
- Vorticity:

  $\omega_x = 0, \omega_y = -\frac{\partial V_z}{\partial x}, \omega_z = \frac{\partial V_y}{\partial x}$, at $x = 0$ and 1;

  $\omega_x = \frac{\partial V_z}{\partial y}, \omega_y = 0, \omega_z = -\frac{\partial V_x}{\partial y}$, at $y = 0$;

  $\omega_x = -\frac{\partial V_y}{\partial z}, \omega_y = \frac{\partial V_x}{\partial z}, \omega_z = 0$, at $z = 0$ and 1;

  $\omega_n = 0, \omega_y = -\frac{\partial V_z}{\partial x}, \omega_z = \frac{\partial V_y}{\partial x}$, at $x = 0$ and 1.

- Vector potential:

  $\frac{\partial \psi_x}{\partial x} = \psi_y = \psi_z = 0$ at $x = 0$ and 1;

  $\psi_x = \frac{\partial \psi_y}{\partial y} = \psi_z = 0$ at $y = 0$ and 1;

  $\psi_x = \psi_y = \frac{\partial \psi_z}{\partial z} = 0$ at $z = 0$ and 1.
- Velocity :

  $V_y = \pm \frac{\rho_{nf} \cdot C_{pnf} \cdot k_f}{\rho_f \cdot C_{pf} \cdot k_{nf}} \cdot \mathrm{Re} \cdot \mathrm{Pr}$ on the vertical sides of the moving fin;

  $V_x = \pm \frac{\rho_{nf} \cdot C_{pnf} \cdot k_f}{\rho_f \cdot C_{pf} \cdot k_{nf}} \cdot \mathrm{Re} \cdot \mathrm{Pr}$ on the bottom horizontal side of the moving fin;

  $V_x = V_y = V_z = 0$ on all other walls.

The generated entropy (S'_{gen}) is written by Kolsi et al. [17] as:

$$S'_{gen} = \left\{ \frac{k_{nf}}{T_0^2} \left[\left(\frac{\partial T'}{\partial x'} \right)^2 + \left(\frac{\partial T'}{\partial y'} \right)^2 + \left(\frac{\partial T'}{\partial z'} \right)^2 \right] \right\} + \frac{\mu_{nf}}{T_0} \left\{ 2 \left[\left(\frac{\partial V'_x}{\partial x'} \right)^2 + \left(\frac{\partial V'_y}{\partial y'} \right)^2 + \left(\frac{\partial V'_z}{\partial z'} \right)^2 \right] + \left(\frac{\partial V'_y}{\partial x'} + \frac{\partial V'_x}{\partial y'} \right)^2 + \left(\frac{\partial V'_z}{\partial y'} + \frac{\partial V'_y}{\partial z'} \right)^2 + \left(\frac{\partial V'_x}{\partial z'} + \frac{\partial V'_z}{\partial x'} \right)^2 \right\} \quad (12)$$

The dimensionless local generated entropy (N_s) is written as:

$$N_s = N_{s\_th} + N_{s\_fr} \quad (13)$$

N_{s_th} and N_{s_fr} are respectively the entropy generations due to heat transfer and viscous effect with:

$$N_{s\_th} = \frac{k_{nf}}{k_f} \left[\left(\frac{\partial T}{\partial x} \right)^2 + \left(\frac{\partial T}{\partial y} \right)^2 + \left(\frac{\partial T}{\partial z} \right)^2 \right] \quad (14)$$

and

$$N_{s\_fr} = \varphi_S \frac{\mu_{nf}}{\mu_f} \left\{ \begin{array}{l} 2 \left[\left(\frac{\partial V_x}{\partial x} \right)^2 + \left(\frac{\partial V_y}{\partial y} \right)^2 + \left(\frac{\partial V_z}{\partial z} \right)^2 \right] + \\ \left[\left(\frac{\partial V_y}{\partial x} + \frac{\partial V_x}{\partial y} \right)^2 + \left(\frac{\partial V_z}{\partial y} + \frac{\partial V_y}{\partial z} \right)^2 + \left(\frac{\partial V_x}{\partial z} + \frac{\partial V_z}{\partial x} \right)^2 \right] \end{array} \right\} \quad (15)$$

where $\varphi_S = \left(\frac{\alpha}{l \Delta T} \right)^2 T_0$ is the irreversibility coefficient.

The total dimensionless generated entropy (S_{tot}) is written as:

$$S_{tot} = \int_v N_s dv = \int_v \left(N_{s\_th} + N_{s\_fr} \right) dv = S_{th} + S_{fr} \quad (16)$$

The Bejan number (Be) is defined as:

$$Be = \frac{S_{th}}{S_{th} + S_{fr}} \quad (17)$$

The local Nusselt number at the hot wall (Nu) is defined as follows:

$$Nu = \left(\frac{k_{nf}}{k_f} \right) \frac{\partial T}{\partial n} \quad (18)$$

while, the average Nusselt number (Nu_{av}), on the isothermal walls is expressed by:

$$Nu_{av} = \int_0^L \int_0^1 Nu \cdot dy \cdot dz \tag{19}$$

The mathematical model described above is written using FORTRAN PowerStation 4.0 The control volume method is used to discretize Equations (Equations (2)–(4) and (12)). The central-difference scheme is used for treating convective terms while the fully implicit procedure is used to discretize the temporal derivatives. The resulting nonlinear algebraic equations are solved using the successive relaxation-iterating scheme. The grids are considered uniform in all directions with clustering nodes on boundaries.

3. Validation of the Code and Grid Dependency

The numerical code is validated with the 2D work of Sun et al. [21] (Figure 2), that considered the case of a differentially heated cavity with a driven top-wall and conductive triangular fin in a different location. The tests are done by comparing the flow field and temperature distribution and it is found that the written homemade code shows good agreement with literature. For nanofluids' buoyancy-induced flow, the code was validated by comparing with the study of Jahanshahi et al. [22] (Figure 3). Jahanshahi et al. [22] studied the effect of adding SiO_2 nanoparticles in water as base fluid on heat transfer and flow structure inside a differentially heated square cavity. It can be concluded from this comparison that there is good agreement.

The sensitivity analysis has been performed with various grids. The tests have been performed for the spatial meshes of 61^3, 71^3, 81^3 and 91^3. The average Nusselt number on the hot wall is considered as a sensitive parameter. The results of the analysis with $Ra = 10^5$, V− and $\varphi = 5\%$ are presented in Table 2. The increase in percentage of Nu_{avg} for the grid 91^3 is only 0.149%. Hence considering the computational economy and accuracy, the time step (10^{-4}) and spatial mesh size of 81^3 is selected for all the simulations. The solution is considered acceptable when the following convergence criterion is satisfied for each step of time as

$$\sum_{i}^{1,2,3} \frac{\max\left|\psi_i^n - \psi_i^{n-1}\right|}{\max\left|\psi_i^n\right|} + \max\left|T_i^n - T_i^{n-1}\right| \leq 10^{-5} \tag{20}$$

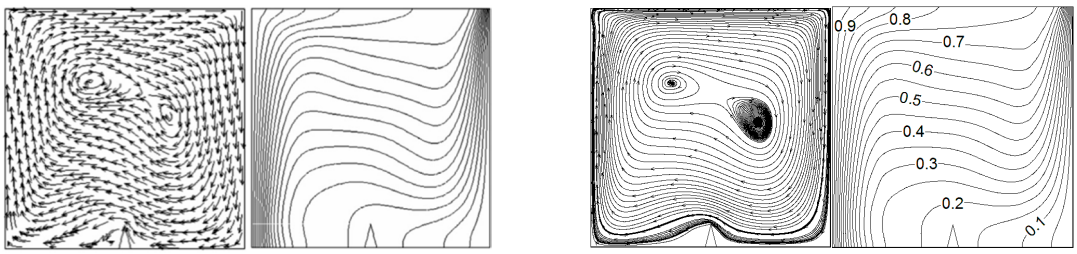

(a) Sun et al. [21] (b) Present results

Figure 2. Validation of the code with 2D solution from the literature for $Ri = 10$; (**a**) study of Sun et al. [21] (on the left) and (**b**) present study (on the right).

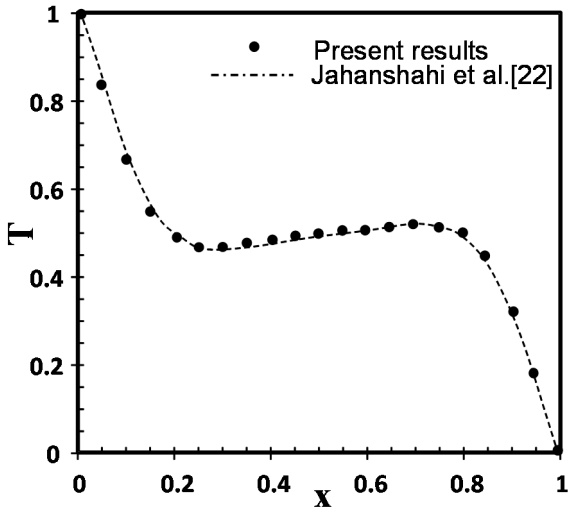

Figure 3. Comparison of the temperature on the axial midline between the present results (cubic closed space; z = 0.5 plane) and results of Jahanshahi et al. [22] (Pr = 6.2, φ = 0.1 and $Ra = 6.2 \times 10^4$).

Table 2. Grid sensitivity analysis; V−, $Ra = 10^5$ and φ = 0.05.

Grid size	Nu_{avg}	Percentage Increase	Incremental Increase
$\mathbf{61^3}$	2.512	-	-
$\mathbf{71^3}$	2.645	5.302	-
$\mathbf{81^3}$	2.686	6.921	1.537
$\mathbf{91^3}$	2.69	7.081	0.149

It should be noted that the results are present for high concentrations, as much as 15%, to make the variations in the heat transfer rate more visible. It should be assumed that the nanofluids remain Newtonian, so the governing equations are the same.

4. Results and Discussion

The governing parameters used to conduct computations are as follows: Rayleigh number ($10^3 \leq Ra \leq 10^5$), Prandtl number (Pr = 6.2), nanoparticle volume fraction ($0 \leq \varphi \leq 0.15$), Reynolds number (Re = 0 for "V = 0" case and Re = 100 for "V+" and "V−"cases) and the irreversibility coefficient ($\varphi_s = 10^{-5}$). Results have been presented in term of flow structure, temperature field, generated entropies and the Nusselt number.

Figure 4 illustrates the flow behavior for $Ra = 10^5$, for (V−), (V = 0) and (V+) cases and different values of carbon nanotube (CNT) concentrations (φ = 0 and φ = 0.15). It is clear that the flow is fully disrupted in the case (V−); in fact, the flow is bypassed by the baffle that moves in the opposite direction of the spontaneous movement of the fluid inside the differentially heated cavity. It becomes obvious, therefore, that the flow becomes multicellular and characterized by the existence of secondary eddies near the top corners of the driven baffle which are known as downstream and upstream secondary eddies. Especially for higher CNT concentration, lower secondary eddies are also revealed near the bottom wall. However, when the baffle is fixed, the flow is stratified horizontally near the bottom wall and vertically near the active walls and characterized by a major clockwise vortex occupying most of the enclosure. The vortex body comprises two cores which are located in the lower part of the cavity compared to the case (V+) where they are located on either side of the driven baffle. These results are more tangible from Figure 5 representing the velocity vector projection in the XY-plane.

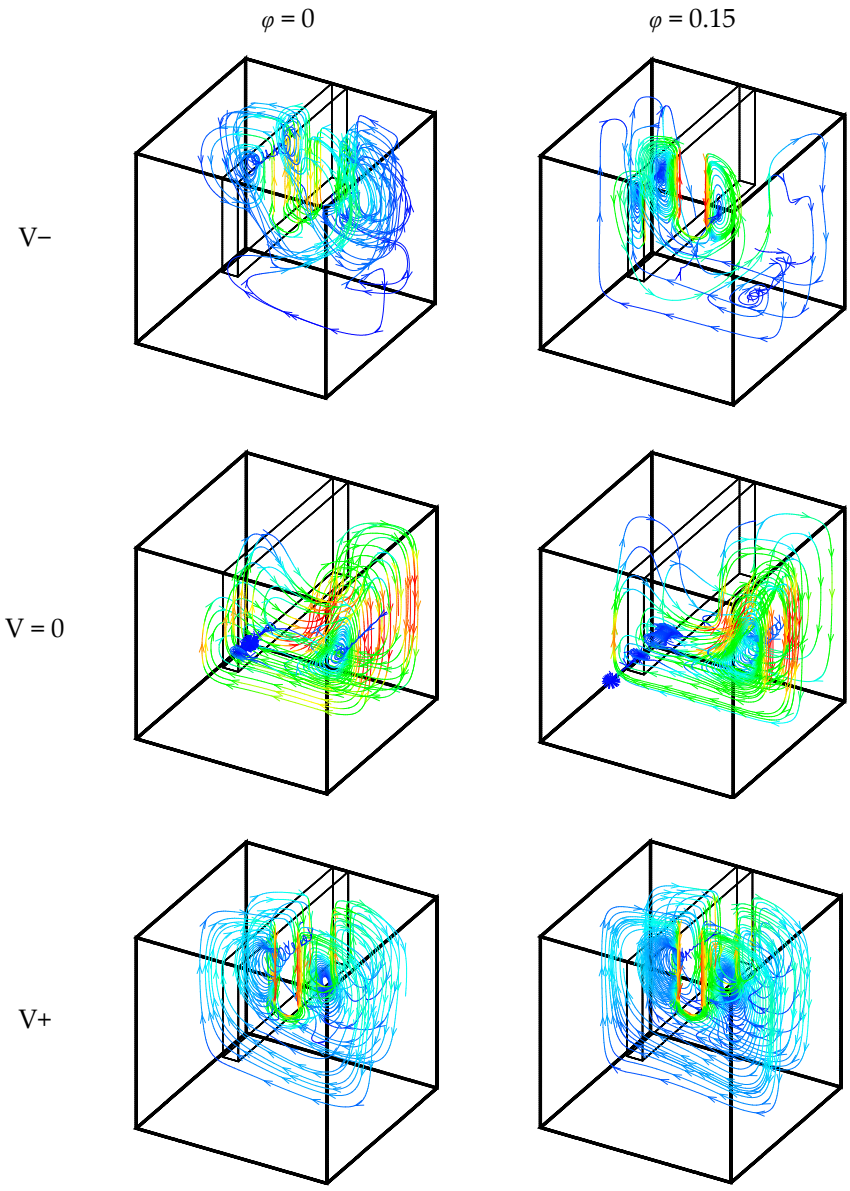

Figure 4. Some particles trajectory for $Ra = 10^5$.

Figure 6 shows the iso-surfaces of temperature for $Ra = 10^5$, and different values of carbon nanotube (CNT) concentrations ($\varphi = 0$ and $\varphi = 0.15$). As it can be seen from this figure, the structure of the iso-surfaces of temperature is extremely affected by the motion of the driven baffle and its direction. However, when the baffle is fixed, the flow is vertically stratified at the lower part of the hot wall and the upper part of the cold wall while it is laminated obliquely at the central portion of the cavity. It is noticed that the distortions at the core of the cavity are more pronounced for the "V+" case due to the cooperation between the buoyancy forces and the displacement of the baffle (the reverse is true for the case "V−"). The effect of adding nanoparticles is also found to increase this distortion for all cases due to heat transfer enhancement.

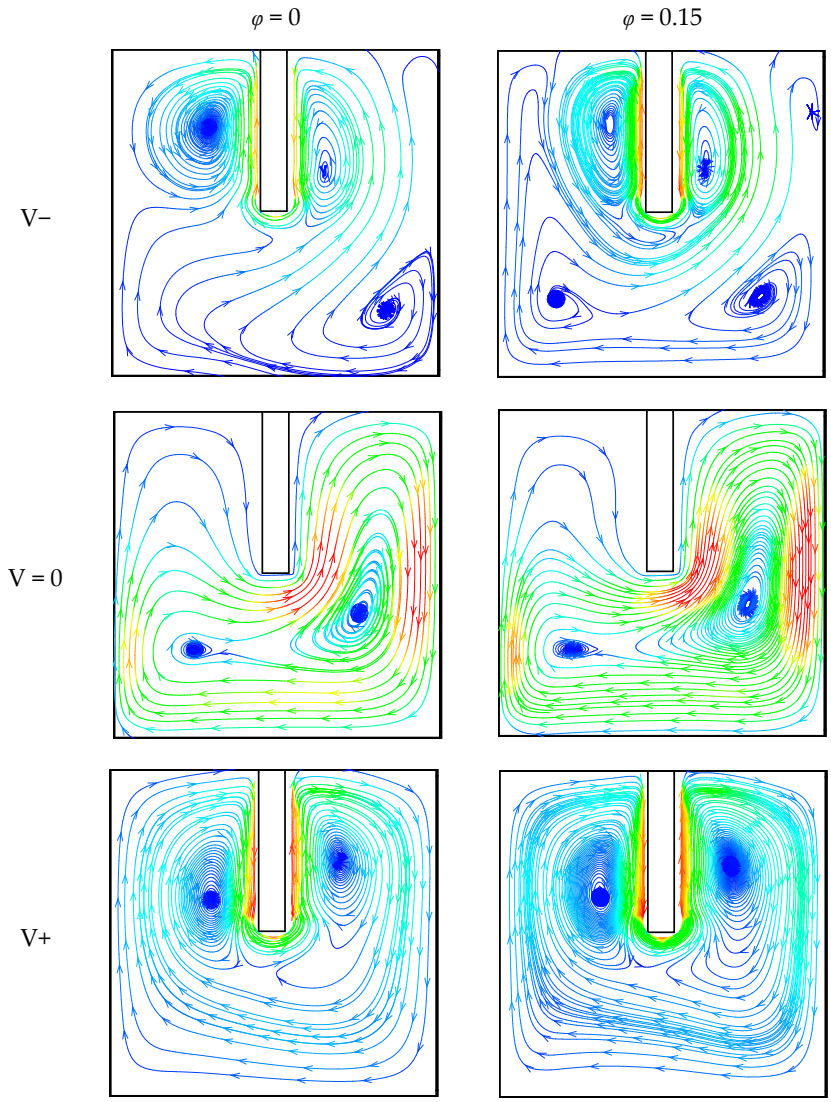

Figure 5. Velocity vector projection at $z = 0.5$ plan for $Ra = 10^5$; (**Left**) $\varphi = 0$; (**Right**) $\varphi = 0.15$.

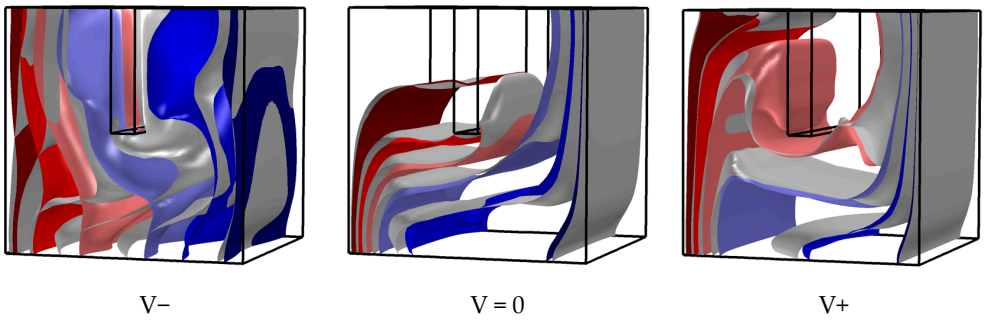

Figure 6. Iso-surfaces of temperature for $Ra = 10^5$ (Gray: $\varphi = 0.15$; Colored: $\varphi = 0$).

Figure 7 depicts isotherms at the $z = 0.5$ plane to see the effects of the nanofluid volume fraction at different baffle velocities. However, the fluid flows when the lid moves in a different direction and the heat transfer mode changes to convection even at the same value of Rayleigh number which is taken as $Ra = 10^5$ for all cases. It is noticed that the effects of the nanofluid volume fraction for moving baffle are more pronounced than that for a fixed baffle. The structure of the isotherms is more disturbed for the case "V−" because of the opposition of the convection motion and that of the baffle and the case of

"V+" is found to accelerate the flow in the direction of decreasing the temperature gradients, especially for the highest nanofluid volume fraction.

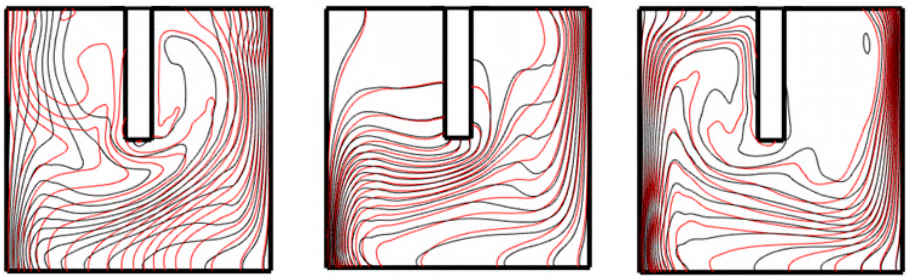

Figure 7. Iso-temperatures at $z = 0.5$ plane for $Ra = 10^5$ (Black: $\varphi = 0.15$; Red: $\varphi = 0$).

The average Nusselt number at the hot wall versus the nanoparticle volume fraction is given in Figure 8 for different Rayleigh numbers and situations of the moving baffle. For all cases, the average Nusselt number is a linear function of the nanoparticle volume fraction. It should be noted that, for a lower Rayleigh number ($Ra = 10^3$), the average Nusselt number is almost constant with variation of the nanofluid volume fraction. For $Ra = 10^4$, the average Nusselt number is increased almost linearly with the increasing nanoparticle volume fraction for both cases of "V+" and V = 0 due to the increasing thermal conductivity of the nanofluids. However, it decreases for the case of "V−" due to the resistance to the spontaneous flow from the hot wall to the cold one caused by the rotational motion of the baffle in the opposite direction. Moreover, it is observed that, by increasing the Rayleigh number, the mean Nusselt number continues to decrease for the case of "V−". Obviously, the highest heat transfer occurred for the case of "V+" and for the highest value of Rayleigh number. It is indeed an interesting result that the rotation direction of the driven baffle can be a control parameter of the heat transfer rate.

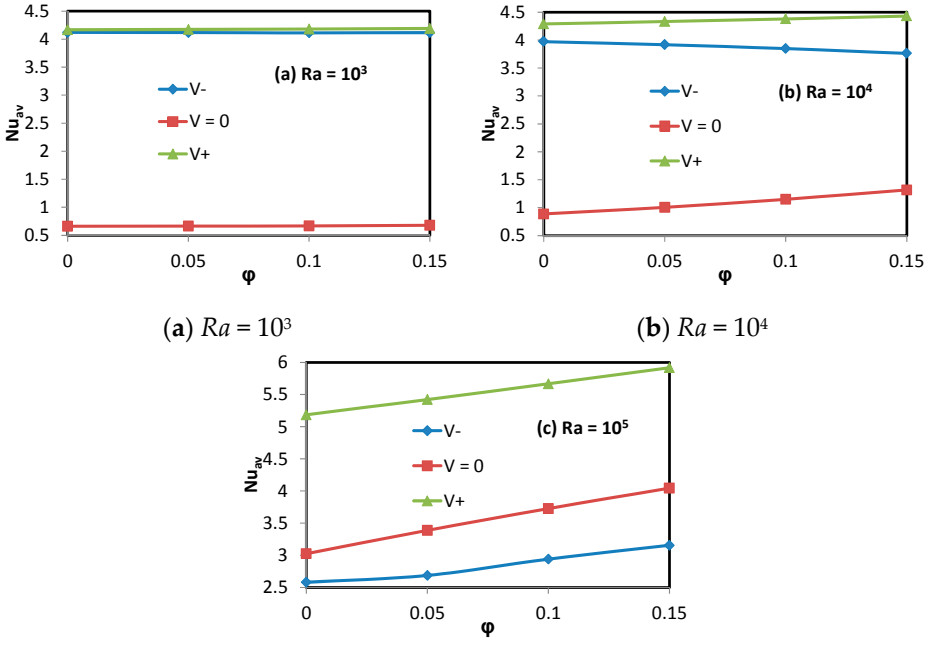

(**a**) $Ra = 10^3$ (**b**) $Ra = 10^4$

(**c**) $Ra = 10^5$

Figure 8. The average Nusselt number at the hot wall as a function of φ for different Ra: (**a**) 10^3; (**b**) 10^4; (**c**) 10^5.

Entropy generation is calculated via the obtained values of temperature and velocities. Thus, local entropy generation due to heat transfer is presented in Figure 9 for different cases and nanofluid volume fractions for $Ra = 10^5$. As shown from the figure, the edge of the baffle becomes less effective on entropy generation for V = 0. The accumulation of the entropy contours is at the lower part of the hot wall and the upper part of the cold wall. Moreover, the increase of the nanofluid volume fraction is accompanied by an increase of the developed thermal entropy. However, when the baffle is driven (case V+), the accumulation of the entropy contours spreads over all the active walls and the effect of the nanofluid volume fraction is more perceptible for the case of "V−" for which contours invade the major part of the cavity. It means that flow entrainment becomes a very effective parameter on entropy generation.

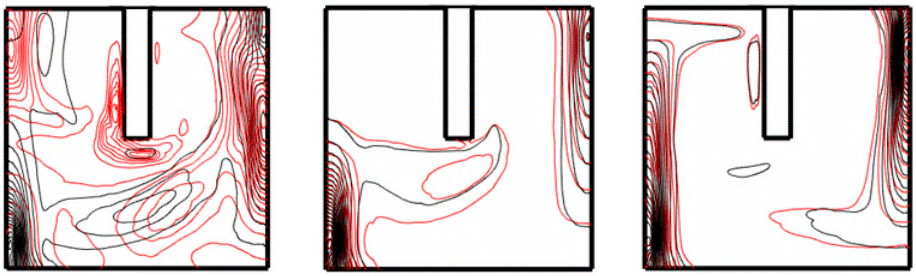

Figure 9. Local thermal entropy generation (S_{th}) at $z = 0.5$ plane for $Ra = 10^5$ (black: $\varphi = 0.15$, red : $\varphi = 0$).

Similarly, Figure 10 illustrates the local entropy generation due to friction at the $z = 0.5$ plane for different cases and $Ra = 10^5$. For driven baffle and regardless of the motion direction, the edge of the baffle is effective on local entropy generation and contours are located only around the baffle. However, for V = 0, active walls and the bottom participate in entropy production.

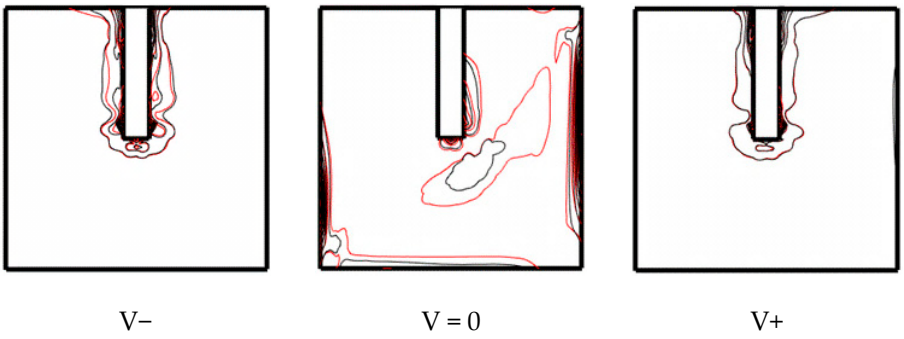

Figure 10. Local entropy generation due to friction (S_{fr}) at $z = 0.5$ plane for $Ra = 10^5$ (black: $\varphi = 0.15$, red: $\varphi = 0$).

Figure 11 displays the local total entropy generation for the same cases as in Figures 9 and 10 to make a comparison. Figure 12 shows the entropy generation due to heat transfer versus the nanoparticle volume fraction at different Rayleigh numbers and different cases of the baffle. For all cases, an increase of the nanofluid volume fraction is accompanied by an increase in the thermal entropy generation. The same observation can be drawn when increasing the Rayleigh number value except the case of "V−"for which the contrary is found. The highest value of entropy generation due to heat transfer is observed for the case "V+" and the highest value of the Rayleigh number.

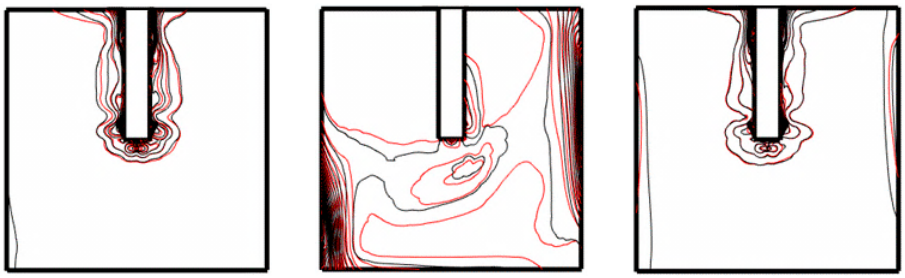

Figure 11. Local total entropy generation (S_{tot}) at $z = 0.5$ plane for $Ra = 10^5$ (black: $\varphi = 0.15$, red: $\varphi = 0$).

In the same way, Figure 13 illustrates the entropy generation due to fluid friction versus the nanoparticle volume fraction at different Rayleigh numbers and different cases of the baffle. This figure shows that the entropy generation is dominated by generation due to fluid friction which prevails over that which is due to the transfer of heat. When the baffle is fixed (V = 0), a small linear increase is obtained for a higher Rayleigh number while it is almost constant for the lower value of Rayleigh number. As seen from the figure, the addition of nanoparticles decreases the entropy generation due to friction and the highest value is obtained for the case of "V−" which favors the fluid friction against the driven baffle. Also, variation of overall entropy generation with the nanoparticle volume fraction is shown in Figure 14 for three studied situations of the baffle. The effect of the Rayleigh number is also illustrated in this figure. Regardless of the Rayleigh number, when the baffle is driven, a linear decrease of the overall entropy generation is observed with the increase of the nanofluid volume fraction. Also, the rotation direction has no significant effect on the total generated entropy. However, in all cases, the moving lid generates higher entropy than the fixed one.

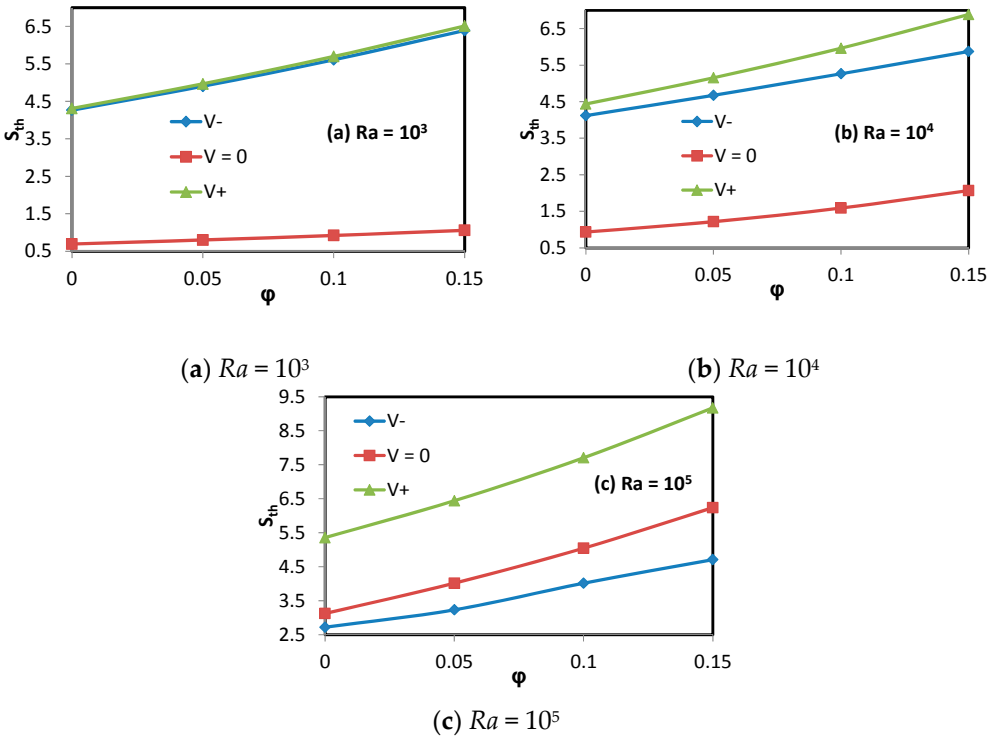

(**a**) $Ra = 10^3$ (**b**) $Ra = 10^4$

(**c**) $Ra = 10^5$

Figure 12. Thermal entropy generation as a function of φ for different Ra: (**a**) 10^3; (**b**) 10^4; (**c**) 10^5.

As mentioned above, the total entropy generation for different nanoparticle volume fractions for different cases and Rayleigh numbers is shown in Figure 14. As expected, the highest values are obtained for case "V−" and the highest value of *Ra* number. However, the value of S_{tot} decreases with the increasing value of the nanoparticle volume fraction except the case of fixed baffle (V = 0) for which S_{tot} value increases almost linearly for $Ra = 10^5$.

Lastly, Figure 15 gives the Bejan number versus the nanoparticle volume fraction for different Rayleigh numbers and different cases of the baffle. As shown from the figure, the Bejan number increases almost linearly with the increasing nanoparticle volume fraction. The highest value of the Bejan number is obtained for the lowest Rayleigh number value ($Ra = 10^3$) and for fixed baffle (V = 0). The effect of the motion direction of the baffle on the Bejan number is significant only for higher values of Rayleigh number. The variation of Bejan has no significance for lower values of Rayleigh number due to the fact that forced convection dominates the natural convection. As defined above, the Bejan number is the ratio of entropy generation due to heat transfer to total entropy generation. Thus, it is almost 1 for the lowest value of Rayleigh number. It means that entropy generation due to fluid friction becomes insignificant in this case.

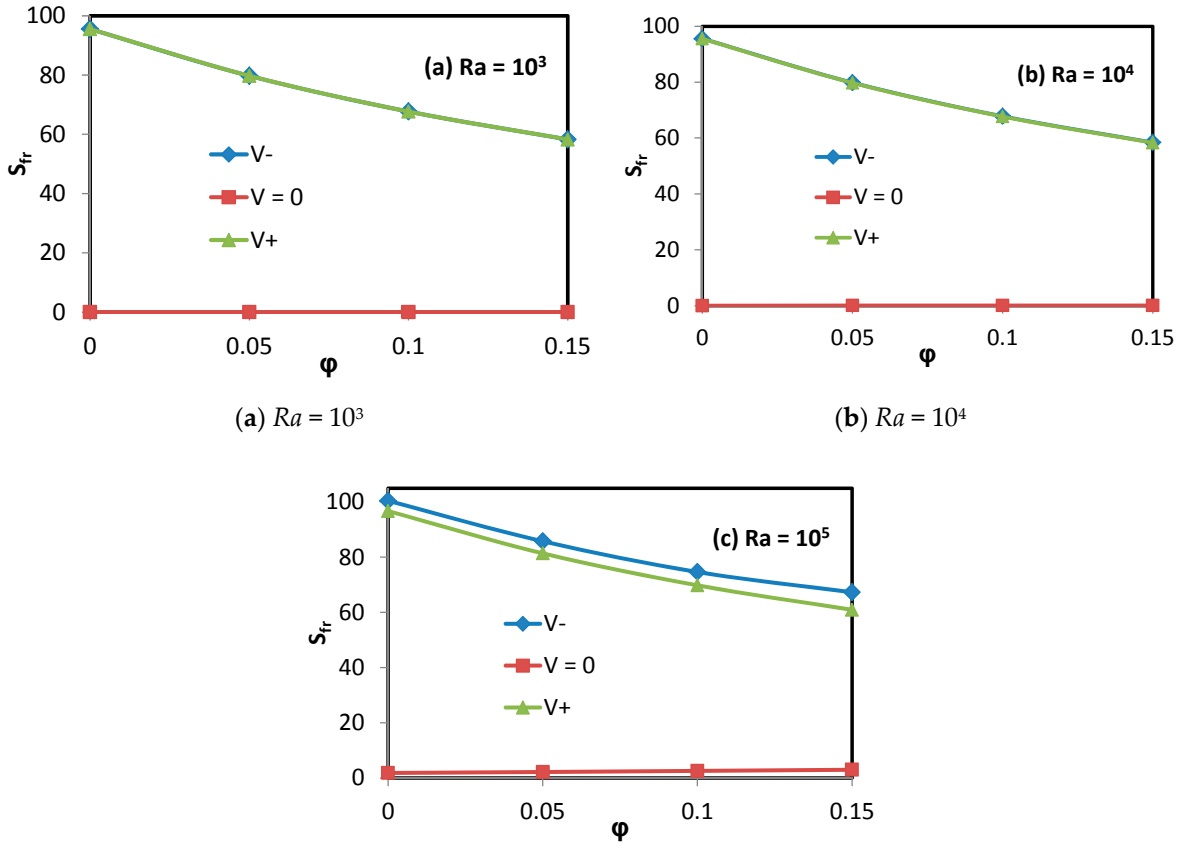

(**a**) $Ra = 10^3$ (**b**) $Ra = 10^4$

(**c**) $Ra = 10^5$

Figure 13. Entropy generation due to friction as a function of φ for different *Ra*: (**a**) 10^3; (**b**) 10^4; (**c**) 10^5.

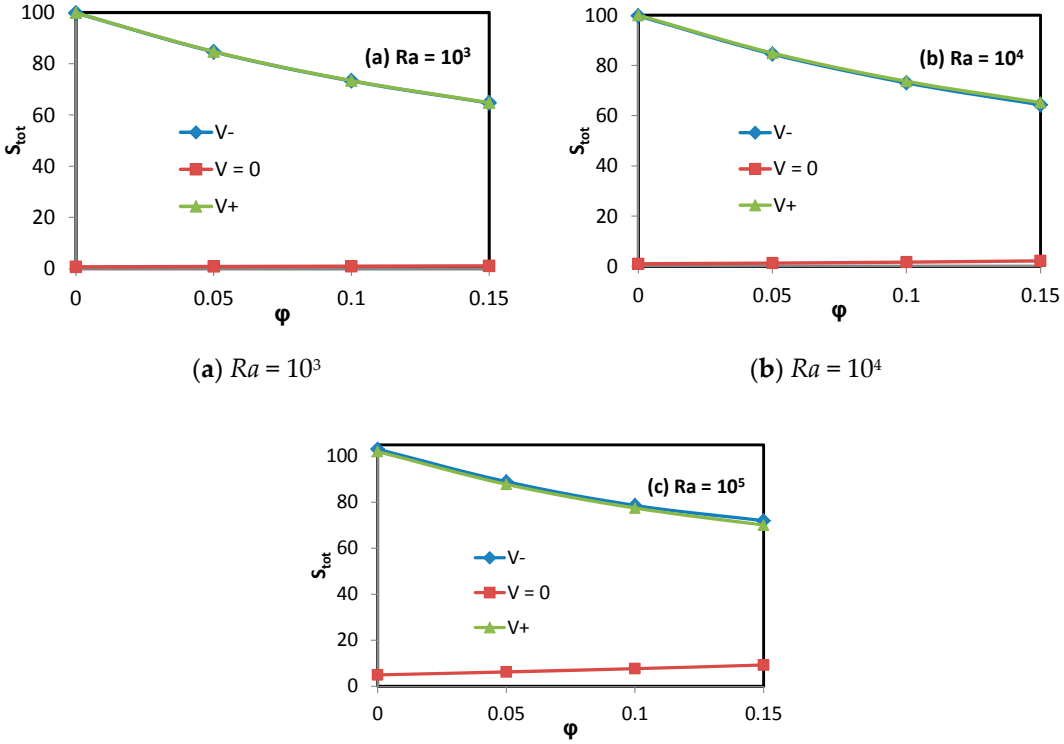

(**a**) $Ra = 10^3$ (**b**) $Ra = 10^4$

(**c**) $Ra = 10^5$

Figure 14. Total entropy generation as a function of φ for different Ra: (**a**) 10^3; (**b**) 10^4; (**c**) 10^5.

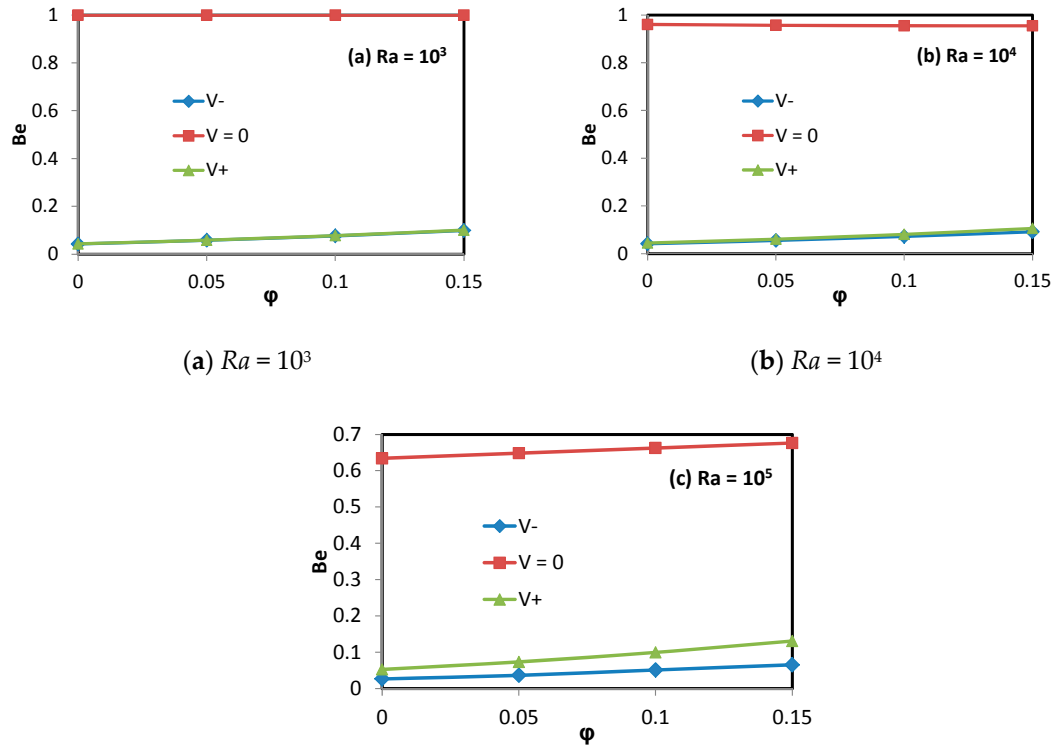

(**a**) $Ra = 10^3$ (**b**) $Ra = 10^4$

(**c**) $Ra = 10^5$

Figure 15. The Bejan number as a function of φ for different Ra: (**a**) 10^3; (**b**) 10^4; (**c**) 10^5.

The behavior of Nu_{av} is shown in Figure 16 as a function of Ri for different nanoparticle volume fractions and different directions in which the baffle is moved. It can be observed that, under the value of Ri = 0.1, the heat transfer rate is nearly constant regardless of both the nanoparticle volume fraction and the baffle motion direction due to negligible buoyancy in the flow. The effect of motion direction is more pronounced when the Richardson number is in the order of unity and the flow is likely to be buoyancy-driven. The case of "V+" is found to enhance the heat transfer, however, the case of "V−", for which the motion direction of the baffles is opposed to that of the flow, induced entropy generation due to friction leading to a decrease in the heat transfer rate. The maximum in Nu_{av} is reached for higher nanoparticle volume fractions with the case of "V+" of driven baffle.

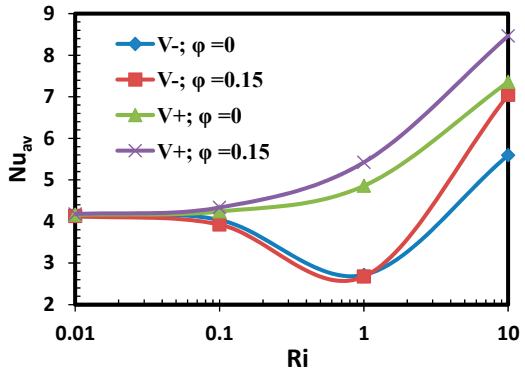

Figure 16. The Nusselt number as a function of *Ri*.

Figure 17 displays changes of the total entropy generation in terms of Ri. As it can be seen, for both motion directions there is only a slight variation in the value of S_{tot} which is nearly constant until the Richardson number reaches unity for a fixed nanoparticle volume fraction value. Moreover, for $Ri < 1$, the higher the nanoparticle volume fraction, the lower the total entropy generation. On the other hand, when Ri exceeds unity, there is an increase in the value of S_{tot} in all cases due to an intensification of natural convection when buoyancy is dominant and there is insufficient kinetic energy to homogenize the flow. The maximum of total entropy generation occurs for the case of "V−" and the smaller nanoparticle volume fraction.

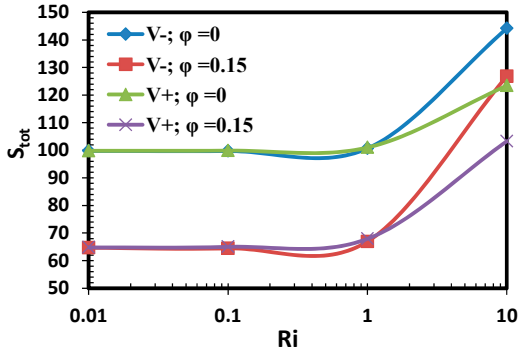

Figure 17. Total entropy generation as a function of *Ri*.

5. Conclusions

A numerical analysis of mixed convection heat transfer in a 3D enclosure filled with CNT-water nanofluid and equipped with adiabatic-driven baffle was performed using computational fluid dynamics (CFD). Some conclusions can be drawn as follows:

1. Driven baffle direction plays an important role in enhancing heat transfer and can be the main parameter to control the desired rate.
2. Adding a low concentration of nanoparticles to pure fluid enhances the heat transfer, especially at high Rayleigh number values.
3. The maximum rate of heat transfer occurred for the case of "V+" and for the highest value of Rayleigh number.
4. The highest values of total generated entropy are obtained for case "V−" and the highest value of *Ra* number.
5. Using moving baffles is not always an efficient technique for enhancing the convective heat transfer at low and moderate Rayleigh number values due to blocking flow at the corners of baffles. It can improve the heat transfer only at high Rayleigh number values where natural convection is the dominant mechanism.

Author Contributions: In this paper, Al-Rashed, Kolsi and Mahian conceived and designed the numerical experiments. Kolsi and Aich performed the experiments. Hussein, Borjini and Al-Rashed analyzed the data. Aich, Mahian and Kolsi wrote the paper.

Conflicts of Interest: The authors declare no conflict of interest.

References

1. Hosseini, S.M.; Vafajoo, L.; Salman, B.H. Performance of CNT-water nanofluid as coolant fluid in shell and tube intercooler of a LPG absorber tower. *Int. J. Heat Mass Transf.* **2016**, *102*, 45–53. [CrossRef]
2. Mahian, O.; Kianifar, A.; Kalogirou, S.A.; Pop, I.; Wongwises, S. A review of the applications of nanofluids in solar energy. *Int. J. Heat Mass Transf.* **2013**, *57*, 582–594. [CrossRef]
3. Mahian, O.; Kianifar, A.; Sahin, A.Z.; Wongwises, S. Performance analysis of a minichannel-based solar collector using different nanofluids. *Energy Convers. Manag.* **2014**, *88*, 129–138. [CrossRef]
4. Mahian, O.; Kianifar, A.; Heris, S.Z.; Wen, D.; Sahin, A.Z.; Wongwises, S. Nanofluids Effects on the Evaporation Rate in a Solar Still Equipped with a Heat Exchanger. *Nano Energy* **2017**, *36*, 134–155. [CrossRef]
5. Ashorynejad, H.R.; Hoseinpour, B. Investigation of different nanofluids effect on entropy generation on natural convection in a porous cavity. *Eur. J. Mech. B Fluids* **2017**, *62*, 86–93. [CrossRef]
6. Cianfrini, C.; Corcione, M.; Habib, E.; Quintino, A. Buoyancy-induced convection in Al_2O_3/water nanofluids from an enclosed heater. *Eur. J. Mech. B Fluids* **2014**, *48*, 123–134. [CrossRef]
7. Wang, G.; Meng, X.; Zeng, M.; Ozoe, H.; Wang, Q. Natural convection heat transfer of copper-water nanofluid in a square cavity with time-periodic boundary temperature. *Heat Transf. Eng.* **2014**, *35*, 630–640. [CrossRef]
8. Sheikhzadeh, G.A.; Arefmanesh, A.; Kheirkhah, M.H.; Abdollahi, R. Natural convection of Cu–water nanofluid in a cavity with partially active side walls. *Eur. J. Mech. B Fluids* **2011**, *30*, 166–176. [CrossRef]
9. Selimefendigil, F.; Öztop, H.F. Numerical study of MHD mixed convection in a nanofluid filled lid driven square enclosure with a rotating cylinder. *Int. J. Heat Mass Transf.* **2014**, *78*, 741–754. [CrossRef]
10. Abu-Nada, E.; Chamkha, A.J. Mixed convection flow of a nanofluid in a lid driven cavity with a wavy wall. *Int. Commun. Heat Mass Transf.* **2014**, *57*, 36–47. [CrossRef]
11. Zonta, F. Nusselt number and friction factor in thermally stratified turbulent channel flow under Non-Oberbeck–Boussinesq conditions. *Int. J. Heat Fluid Flow* **2013**, *44*, 489–494. [CrossRef]
12. Zonta, F.; Chibbaro, S. Entropy production and fluctuation relation in turbulent thermal convection. *Europhys. Lett.* **2016**, *114*, 50011. [CrossRef]
13. Ngo, L.; Bello-Ochende, T.; Meyer, J. Numerical modelling and optimization of natural convection heat loss suppression in a solar cavity receiver with plate fins. *Renew. Energy* **2015**, *74*, 95–105. [CrossRef]
14. Ternik, P. Conduction and convection heat transfer characteristics of water–Au nanofluid in a cubic enclosure with differentially heated side walls. *Int. J. Heat Mass Transf.* **2015**, *80*, 368–375. [CrossRef]
15. Zhang, Z.; Chen, W.; Zhu, Z.; Li, Y. Numerical exploration of turbulent air natural convection in a differentially heated square cavity at Ra = 5.33×10^9. *Heat Mass Transf.* **2014**, *50*, 1737–1749. [CrossRef]
16. Aich, W.; Kolsi, L.; Borjini, M.N.; Aissia, H.B.; Öztop, H.F.; Abu-Hamdeh, N. Three-dimensional CFD Analysis of Buoyancy-driven Natural Ventilation and Entropy Generation in a Prismatic Greenhouse. *Therm. Sci.* **2016**, *00*, 52. [CrossRef]

17. Kolsi, L.; Mahian, O.; Öztop, H.F.; Aich, W.; Borjini, M.N.; Abu-Hamdeh, N.; Aissia, H.B. 3D Buoyancy-Induced Flow and Entropy Generation of Nanofluid-Filled Open Cavities Having Adiabatic Diamond Shaped Obstacles. *Entropy* **2016**, *18*, 232. [CrossRef]
18. Kahveci, K. Buoyancy driven heat transfer of nanofluids in a tilted enclosure. *J. Heat Transf.* **2010**, *132*, 062501. [CrossRef]
19. Xue, Q.Z. Model for thermal conductivity of carbon nanotube-based composites. *Phys. B Condens. Matter* **2005**, *368*, 302–307. [CrossRef]
20. Mahian, O.; Kianifar, A.; Kleinstreuer, C.; Moh'd, A.A.; Pop, I.; Sahin, A.Z.; Wongwises, S. A review of entropy generation in nanofluid flow. *Int. J. Heat Mass Transf.* **2013**, *65*, 514–532. [CrossRef]
21. Sun, C.; Yu, B.; Oztop, H.F.; Wang, Y.; Wei, J. Control of mixed convection in lid-driven enclosures using conductive triangular fins. *Int. J. Heat Mass Transf.* **2011**, *54*, 894–909. [CrossRef]
22. Jahanshahi, M.; Hosseinizadeh, S.F.; Alipanah, M.; Dehghani, A.; Vakilinejad, G.R. Numerical simulation of free convection based on experimental measured conductivity in a square cavity using Water/SiO_2 nanofluid. *Int. Commun. Heat Mass Transf.* **2010**, *37*, 687–694. [CrossRef]